Correlation of Microstructure and Fatigue Crack Growth Resistance in Ti-6Al-4V alloy

Stephen Masete,[1,2*] Kalenda Mutombo[1,2*], Roelf Mostert[2], Charles Siyasiya[2] and Waldo Stumpf[2]

[1]MSM/Light Metals, Council for Scientific and Industrial Research, (CSIR), Pretoria, South Africa
[2]Department of Materials Science and Metallurgical Engineering, University of Pretoria, Pretoria, South Africa

[*]Email: smasete@csir.co.za, kmutombo@csir.co.za

The effect of the microstructure on fatigue crack growth resistance of the Ti-6Al-4V alloy was investigated. Various microstructures were produced by solution treatment above the beta transus temperature followed by cooling at different rates. The compact tension specimen was used to measure fatigue crack growth rate and to determine the Paris constants. The lamellar microstructural morphology showed a better fatigue crack growth resistance than the fully martensitic microstructure. The threshold stress intensity and the critical stress intensity factors were higher for the lamellar morphology (ΔK_{th} = 15.2, K_c = 68) but lower for the fully martensitic morphology (ΔK_{th} =11.6, K_c = 63). Random orientation of the α/β colonies in the lamellar microstructure led to crack branching and formation of secondary cracks. The fully martensitic morphology had cleavage fractures leading to a smoother fracture surface. Furthermore, the presence of brittle and fine martensitic needles could not hinder the crack propagation.

INTRODUCTION

Rotating aircraft engine parts suffer mainly from fatigue failures caused by vibrations and start-stop cycles (Inagaki 2014; Nalla et al. 2002; Lütjering & Williams 2007). The front part of the engine where operating temperatures are lower than 300°C, uses the Ti-6Al-4V alloy for the fan blades. The fan blades experience fatigue loading of high frequencies and varying stress ratios. Fatigue crack initiation, crack propagation as well as crack growth in such Ti-6Al-4V alloy parts are of interest in the design of durable structures. The common method of assessing fatigue life is using the stress and a number of cycles (S-N) curve and investigating the crack initiation and propagation. The S-N curve method would not apply where a structure has a pre-existing crack. The fracture mechanics approach becomes useful in determining the threshold stress intensity required to cause an existing crack to propagate. The determination of the fatigue crack growth rate and fracture toughness properties are crucial for structures with pre-existing cracks.

The role of bimodal, equaixed or lamellar microstructures on fatigue crack initiation and growth rate has been well documented (Nalla et al. 2002; Benedetti & Fontanari 2004) . The lamellar morphology is known to have a higher fatigue crack growth resistance than the equiaxed or bimodal morphology. These microstructures are produced mainly from solution treatment and thermomechanical processes either below or above the β-transus without any ageing treatment. Enhanced fatigue crack growth behaviour is required without compromising tensile properties of components. Solution treatment above the β-transus followed by ageing has been shown to result in improved tensile strength.

However, the role of ageing treatment in the optimisation of fatigue crack growth behaviour is not well covered. Developing an understanding of the correlation between the microstructural morphology and the fatigue crack growth mechanism would assist in the development of durable aerospace parts with better fatigue crack growth resistance.

Therefore, the current work investigates the role of various microstructural morphologies produced by solution treatment above the β transus treatment on fatigue crack growth rate in the Ti-6Al-4V alloy.

EXPERIMENTAL PROCEDURE

The wrought commercial, grade 23 Ti-6Al-4V ELI, received as forged rods of 74 mm in diameter, was used. The material's chemical specification is shown in Table 1.

Table I. Chemical composition of the as received Ti-6Al-4V ELI alloy

Alloying elements (weight %)								
Ti	Al	V	Fe	C	N	O	H	Residual elements
balance	6.38	4.23	0.15	<0.01	0.01	0.1	0.002	<0.40

The solution treatment temperature above the beta (β) transus temperature (1050°C) was chosen to totally convert the Ti-6Al-4V's initial phases to the single β-phase before cooling. The effects of crystallographic texture from rolling or forging on mechanical properties will also be eliminated by solution treatment above the β transus temperature. (Al-Bermani et al. 2010; Lütjering & Williams 2007; Peters 2003).

The as received Ti-6Al-4V wrought alloy was cut into 10 mm thick discs and solution treated (ST) at 1050°C for 30 minutes in a Naber N150 muffle furnace. Solution treated specimens were quenched in water (WQ) to produce a fully martensitic morphology or furnace cooled (FC) to produce a colony lamellar morphology. The WQ cooling rate was approximated to 400°C/second while the furnace cooling rate was 400°C/hour. Specimen preparation for heat treatment and microstructural analysis is shown schematically in Figure 1.

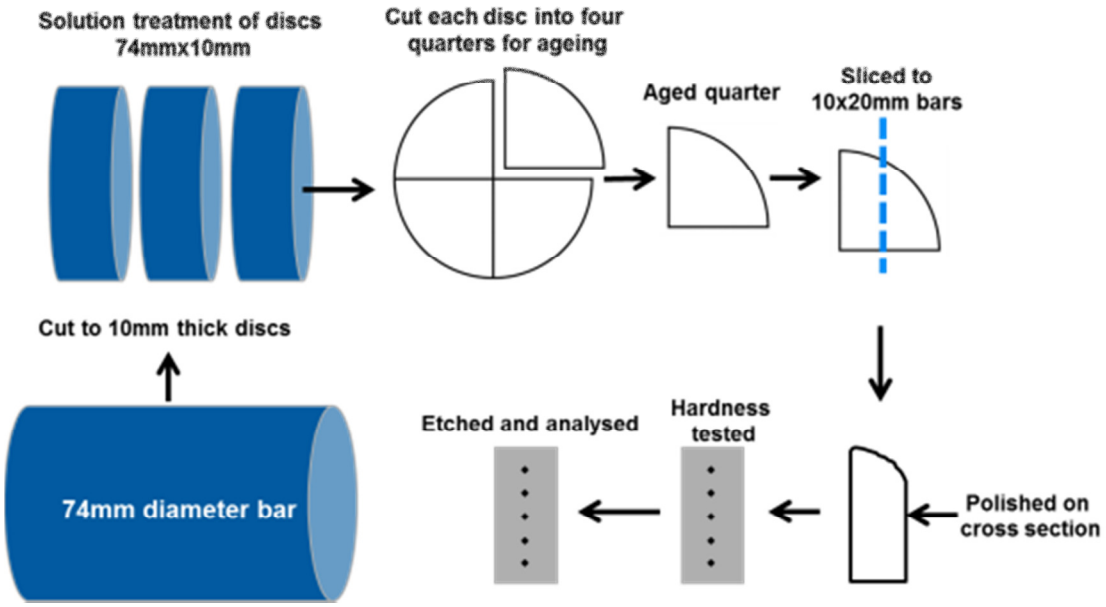

Figure 1. Sample preparation for heat treatment, microstructural analysis and hardness measurements

Sample Preparation

All heat treated specimens were sectioned to remove the alpha-case and hot mounted in Bakelite resin using an ATM Opal 450 mounting press. The specimens were ground and polished using an ATM Saphir 550 polisher and were thereafter cleaned in the ultrasonic bath using ethanol for about 10 minutes and then air dried. Etching was done using Kroll's reagent (1 ml HF + 2 ml HNO3 + 333 ml water) for 20 to 30 seconds.

Microstructural Analysis

A Leica MZ 16A stereo microscope, Leica DMI5000M inverted optical microscope (OM) equipped with image analysis software (Image Pro Plus) and a Jeol JSM-6510 Scanning Electron Microscope (SEM) equipped with X-ray electron diffraction spectrometry (EDS) were used to investigate the

microstructural changes after the solution treatment.

The beta (β) grain size, α′ lath width, α lath width and α/β content were quantified by the linear intercept method according to the standard (ASTM-E112 2004). Median grain size, standard deviation, and coefficient of variation were calculated for each specimen.

The martensitic (α') lath measurements were performed using SEM micrographs taken at a magnification of 3000x, while for the thickness of the α-laths a magnification of 1000x was used. The measurements of α and β-phase content were only performed on colony lamellar structures.

Hardness measurements

The Vickers macro-hardnesses were obtained with a load of 10 kg according to the standard (ASTM E384 2012) and the median average, standard deviation, and coefficient of variation of 10 individual measurements found.

Fatigue Crack Growth Rate Determination (FCGR)

Bar type compact tension specimens (CT), machined after heat treatment, were used to determine the fatigue crack growth rate (FCGR) using an Instron™ 1342 tensile tester. A 20 mm thick specimen was heat treated, followed by machining off 2.5 mm layers on both sides to remove the oxide layer. Compact tension specimens with a final thickness (B), width (W) and height (H), as shown in Figure 2, were machined according to the standard (ASTM Standard E647 − 13a 2014).

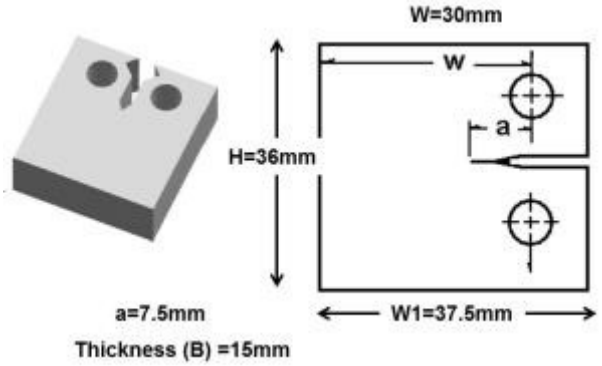

Figure 2: Thickness (B), width (w) and height (H) of the bar type compact tension specimen.

The CT specimens were polished on both sides to a mirror like finished surface to aid in crack observation during testing. A 7.5 mm starter notch was introduced using wire cutting and a crack opening displacement (COD) gauge was used to monitor the fatigue crack growth. Room temperature FCGR tests were done at a constant delta load amplitude (ΔP) of 8000 N, which had a sine waveform with a cyclic load ratio (P_{min}/P_{max}) of 0.1 and a frequency of 15 Hz. The crack length (a) was measured using the compliance method, while the number of cycles (N) and change in load (ΔP) were recorded. The fatigue crack growth rate (da/dN) and change in stress intensity (ΔK) were determined using the secant method according to the Standard ASTM E647.

A plot of crack length (*a*) versus the number of cycles (N) was produced. A Paris curve showing the fatigue crack growth rate versus change in stress intensity was also generated by plotting da/dN versus ΔK on semi- logarithmic scale as per Equation [1]. The Paris constants, *C*, and *m*, which are related to material variables and test conditions, were determined from the straight line region of the Paris curve by plotting $\log\frac{da}{dN}$ against log(ΔK) according to Equation [2].

$$\frac{da}{dN} = C(\Delta K)^m \quad [1]$$

$$\log\frac{da}{dN} = \log C + m\log(\Delta K) \quad [2]$$

The value of the threshold stress intensity, ΔK_{th}, needed to be determined at the da/dN values of 10^{-10} to 10^{-8} m/cycle according to the standard (ASTM Standard E647 − 13a 2014). However, the da/dN

values of the Ti-6Al-4V alloy of this study were greater than 10^{-8} m/cycle. The ΔK_{th} values were then reported as the lowest ΔK values recorded where the crack started to propagate. The critical stress intensity, K_c, was read off from the raw data as the highest recorded ΔK values during the test.

Optical and scanning electron microscopy were used to perform fractographic studies of fractured specimens after fatigue testing.

RESULTS

The microstructure of the as received Ti-6Al-4V is shown in the SEM micrograph in Figure 3. The structure consisted of globular primary α-phase shown as dark areas surrounded β-phase (bright areas). The average grain size of the as received alloy was about 8 µm and its hardness was 310 ±5.6 HV_{10}.

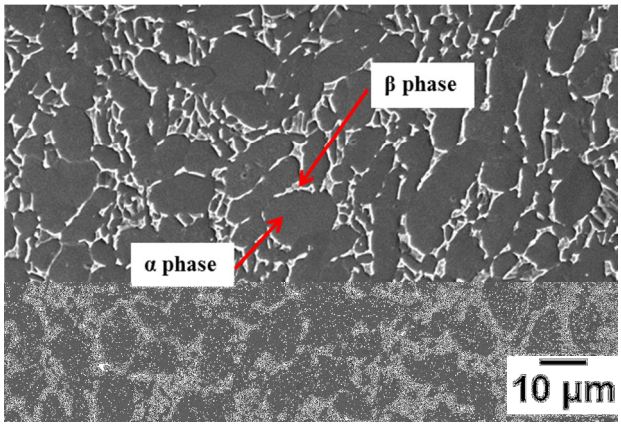

Figure 3: a and β-phase in the as received Ti-6Al-4V alloy.

Solution treated and water quenched Ti-6Al-4V specimens produced a fully martensitic morphology as shown in Figure 4(a), which consists of fine acicular α′ martensitic needle like phases, while the grain boundaries (GB) consist of the β-phase. A colony lamellar microstructure is shown in Figure 4(b) which is produced by solution treatment followed by furnace cooling. The colony microstructure has grain boundaries of α-phase resulting from complete transformation of β to α-phase. The grains consist of colonies of α and β lamellar structures in which the α-laths are parallel plate like structures having thin β regions sandwiched in between them.

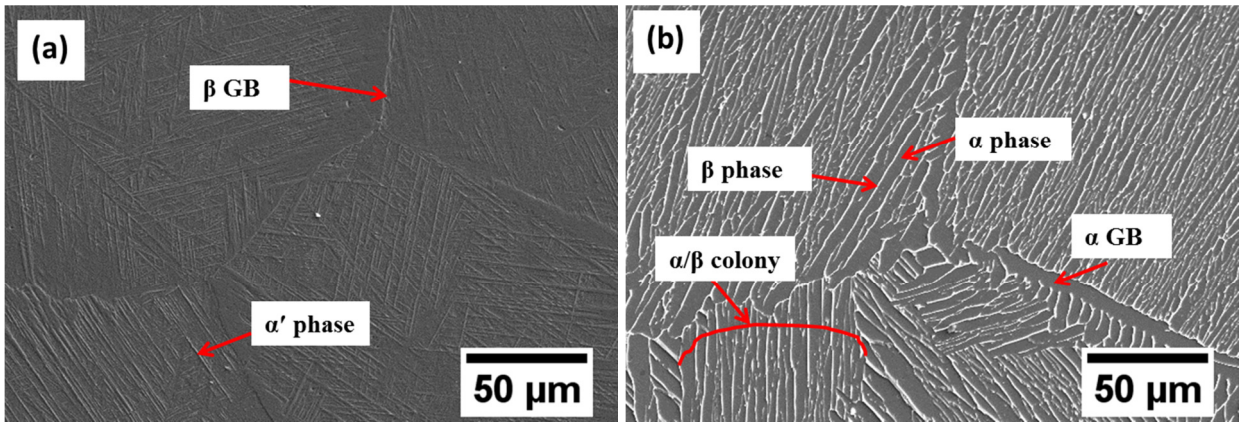

Figure 4: (a) Martensitic (ST/WQ) and, (b) colony lamellar structure (ST/FC) of Ti-6Al-4V alloy

Grain and lath size, α-phase content and hardness results are shown in Table 2. The β grains of the ST/FC specimen are larger than that of the ST/WQ specimens. The martensite laths (α′) are thinner than α laths found in colony morphology. The fully martensitic microstructure has a higher hardness than the colony morphology.

Table 2: Grain and lath size, and a-phase content

Specimen details	β grain size (μm)+/_SD	α content (%)+/_SD	α lath width (μm)+-SD	Hardness, HV_{10} (kg/mm^2)
ST/WQ	713+/-104	-	0.78+/-0.2	356±7
ST/FC	1027+/-196	83+/-3.9	2.94+/-1.4	303±30

Fatigue crack growth rate and Paris constants.

A plot of crack length versus the number of cycles for ST/WQ and ST/FC specimens is shown in Figure 5. The specimen ST/FC show a larger number of fatigue cycles than the ST/ WQ for the same crack length. The ST/WQ sample reaches fast fracture at a lower number of cycles than the STFC sample.

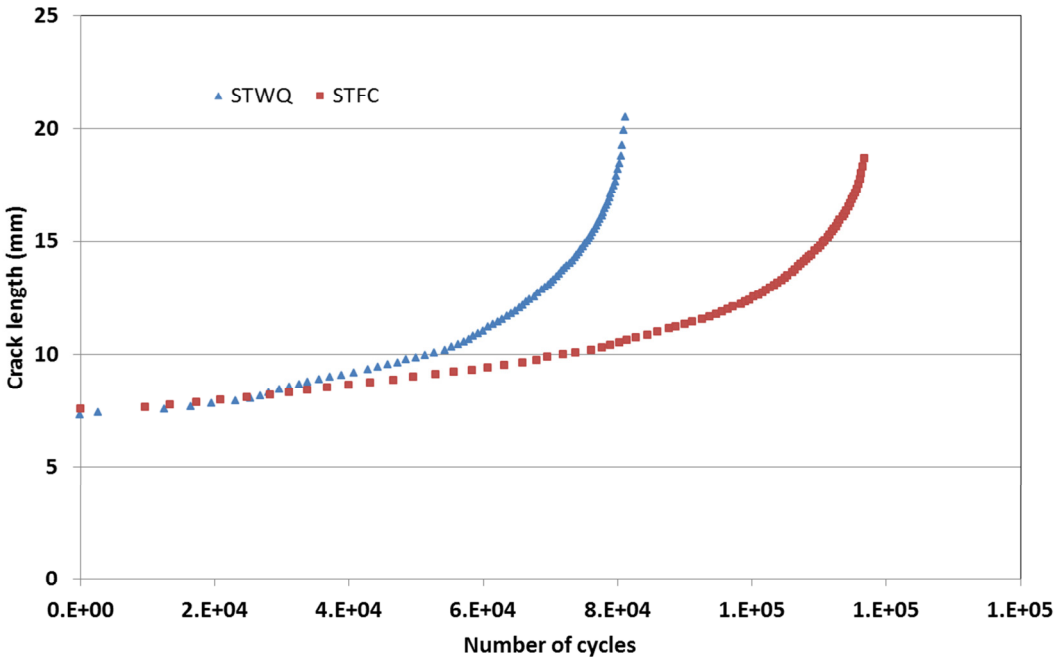

Figure 5: The variation of crack length as a function of a number of cycles of ST/WQ and ST/FC Ti64 specimens.

A Paris curve showing crack growth rate versus ΔK is shown in Figure 6. The ST/FC specimen has better fatigue crack growth resistance than the ST/WQ specimen. The crack growth rate (da/dN) of the ST/WQ microstructure is higher than that of the ST/FC microstructure in the Ti-6Al-4V alloy for ΔK values below 40 $MPa.m^{0.5}$ whereas above this value, the crack propagated at the same rate in both of the ST/QW and ST/FC Ti-6Al-4V specimens.

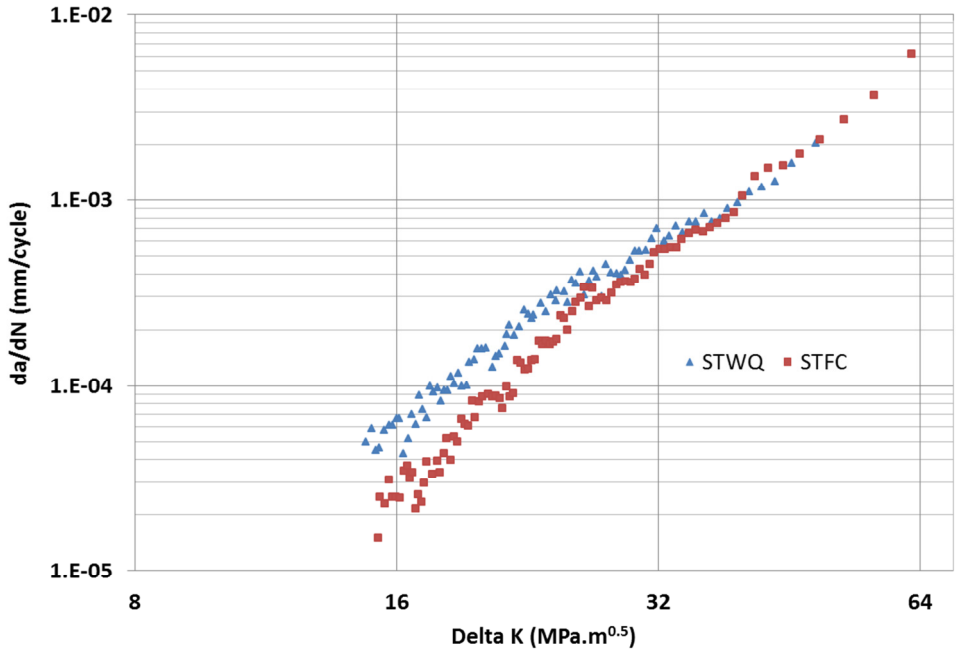

Figure 6: The change in crack growth rate as a function of ΔK of ST/WQ and ST/FC Ti64 specimens

The Paris constants *C*, *m*, ΔK_{th} and K_c were calculated for both ST/WQ and ST/FC specimens and are given in Table 3. The specimen ST/WQ has a higher *C* constant than the ST/FC. The *m* constants are within the expected range for metals, which is between 2 and 4. The threshold stress intensity factor (ΔK_{th}) is lower for the ST/WQ specimen. The critical stress intensity (K_c) value for the ST/WQ is also lower than for the ST/FC specimen.

Table 3: Paris constants of the Ti-6Al-4V alloy

Specimen details	C (mm/cycle)	m	ΔK_{th} (MPa.m$^{0.5}$)	K_c (MPa.m$^{0.5}$)
ST/WQ	$1x10^{-8}$	3.2	11.6±0.5	63±1.9
ST/FC	$4x10^{-10}$	4.0	15.2±0.6	68±1.2

The cross sectional side views of the - fracture topography of the ST/WQ and ST/FC specimens are shown in Figures 7 and 8. The side view of the fractured surface was smoother in the fully martensitic specimen (Figure 7(a)) and more uneven in the lamellar specimen (Figure 7(b)). The ST/WQ specimen shows more straight and smooth fracture surfaces (Figure 8(a)) while the ST and FC specimen (Figure 8(b)) show secondary cracks and crack branching.

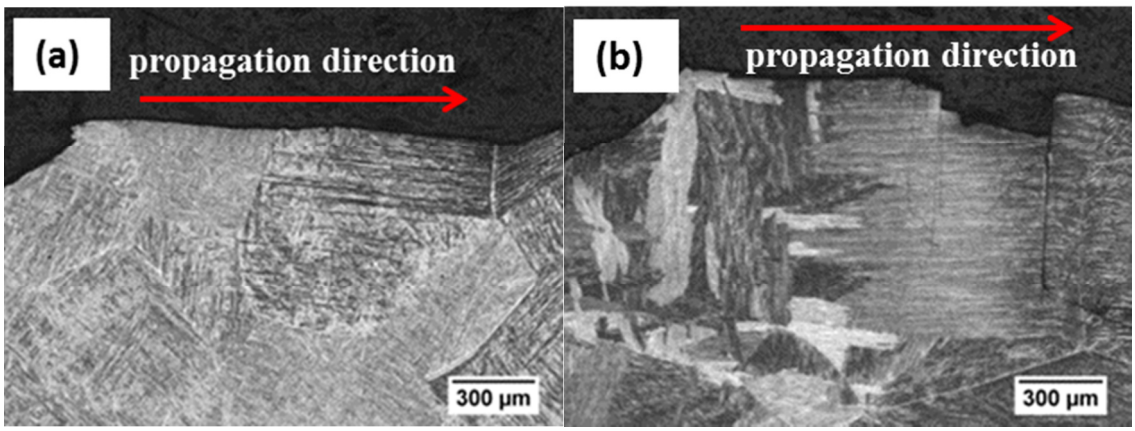

Figure 7: Side view of the crack propagation path in the (a) martensitic (ST/WQ) and, (b) colony microstructure (ST/FC), after fatigue crack growth testing.

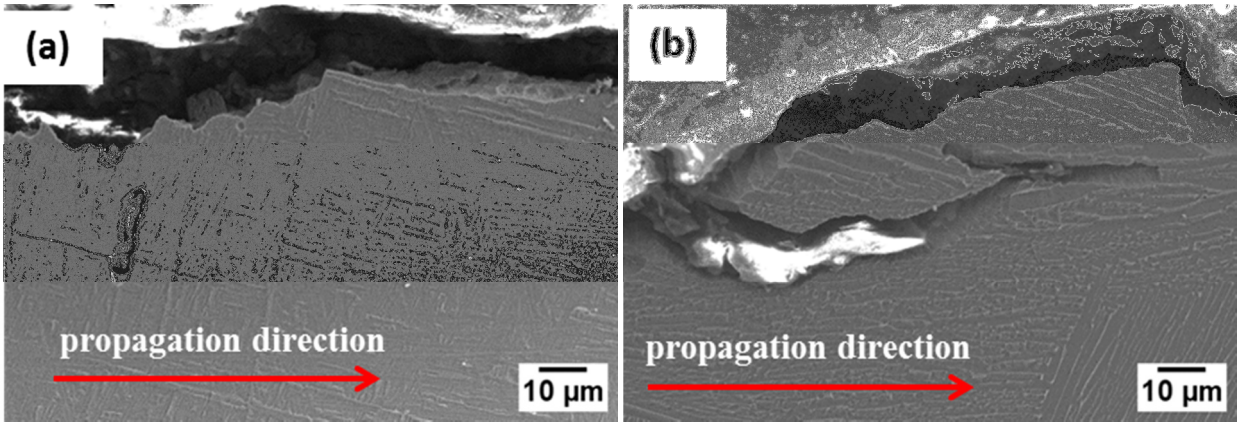

Figure 8: Side view of the crack propagation path in the (a) martensitic (ST/WQ) and, (b) colony microstructure (ST/FC), after fatigue crack growth testing shown at a higher magnification than in figure 8.

Figure 9 shows stereo microscope images of the fracture faces. The fractured surface of the fully martensitic specimen ST/WQ (Figure 9 (a)) shows smoother fractures, while the ST/FC specimen (Figure 11(a)) shows more rough fracture surfaces.

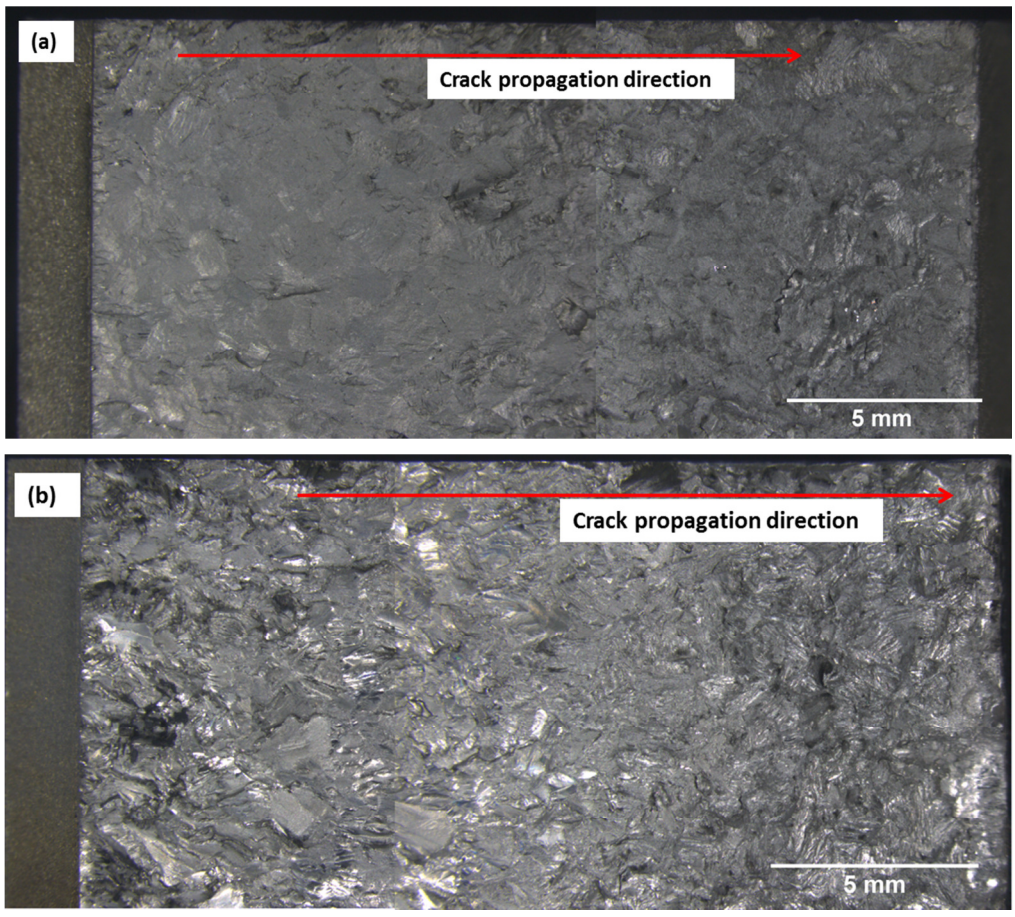

Figure 9: Stereo micrographs of fracture surface in (a) martensitic (ST/WQ) and, (b) colony microstructure (ST/FC), after fatigue crack growth testing.

The SEM fractured surfaces of ST/WQ and ST/FC specimens, revealing the crack initiation area and propagation area, are respectively shown in Figures 10 (a) and (b). There are no obvious defects where the cracks initiated for both specimens.

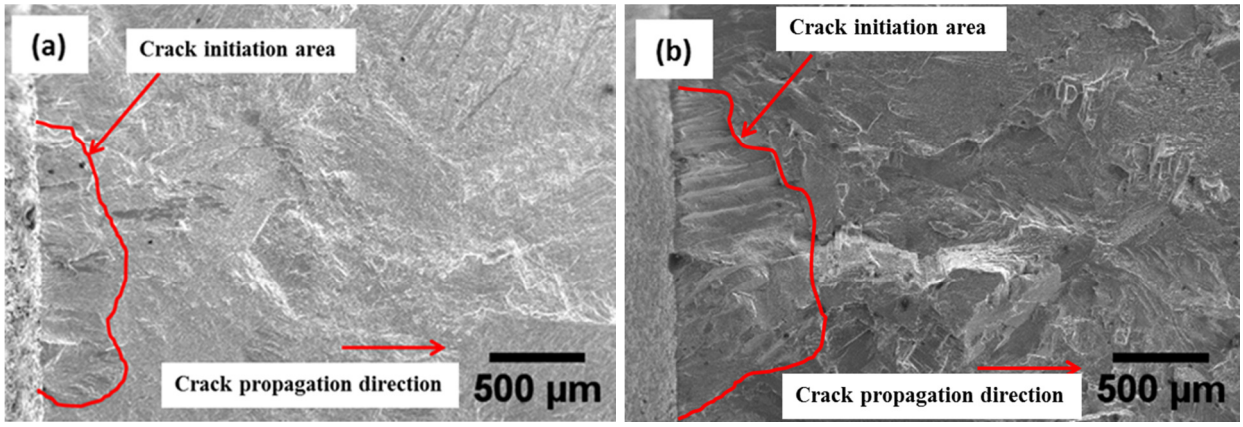

Figure 10: SEM micrographs of the fractured surface showing crack initiation area in (a) martensitic (ST/WQ) and, (b) colony microstructure (ST/FC), after fatigue crack growth testing.

Secondary microcracks initiated during fatigue crack propagation in the ST/WQ and ST/FC specimens are respectively shown in Figures 11 (a) and (b). The secondary microcracks in both structures form parallel to the α' laths and the α/β laths, which is consistent with the propagation direction of secondary cracks observed in Figures 8 (a) and (b). The deflections shown in the martensitic microstructure are smaller than those within the colony microstructure.

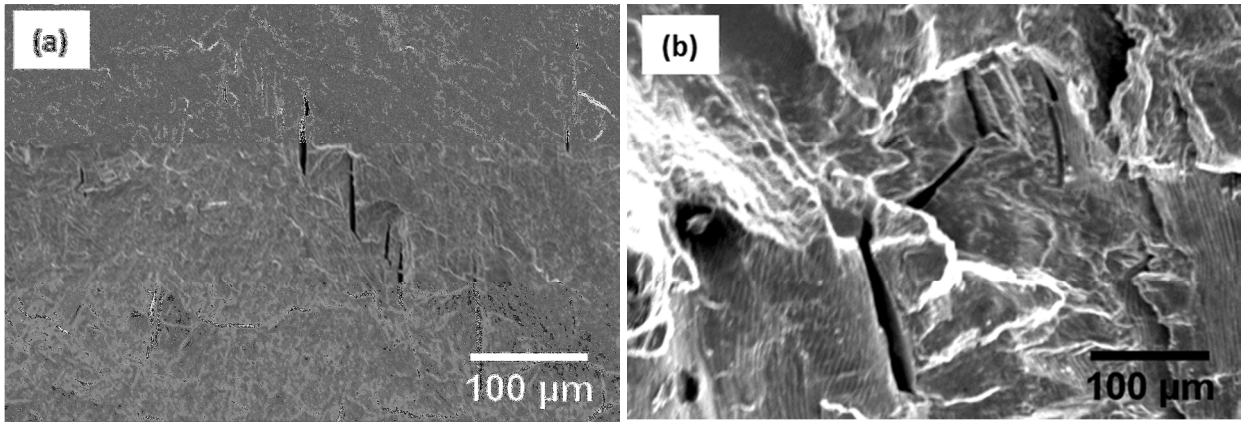

Figure 11: SEM micrographs of the fracture surface showing crack deflection in (a) martensitic (ST/WQ) and, (b) colony microstructure (ST/FC), after fatigue crack growth testing.

DISCUSSION

The high cooling rate (WQ) from the β-phase region (ST at 1050 ^{o}C) reduces the exposure time to diffusion dominated transformation of the β-phase and β grains. The shorter time of ST/WQ led to relatively smaller β grains and a fine lath structure in the Ti-6Al-4V martensite. On the other hand the cooling rate is low in the ST/FC treatment, and the grain size and α/β laths become coarser than in the martensitic microstructure. The fully martensitic morphology gave a higher hardness value than the colony morphology due to the presence of fine martensitic needles. As the thickness of the laths increased in the ST/FC microstructure, the hardness dropped. The hardness results are consistent with the general Hall-Petch relationship where finer structures give higher hardness values. The higher standard deviation in hardness from a colony microstructure indicates heterogeneity of the microstructure as compared to the more homogenous fully martensitic morphology in the ST/WQ structure.

The fatigue cracks in the ST/WQ and ST/FC structures grew almost at the same rate up to about 3.10^4 cycles. It picked up exponentially at about 5.10^4 cycles in the ST/WQ specimen and at about 9.10^4 cycles in the ST/ FC specimen. Obviously, the fatigue crack growth resistance of the lamellar microstructural morphology was higher than that of the fully martensitic morphology. This

observation also implies that a lower stress intensity was required to propagate a crack in a fully martensitic morphology than within a lamellar morphology. Crack propagation in both Ti-6Al-4V microstructures is controlled by the grain size, sub-grains or colonies and the size and orientation of α/β lamellae. A crack will propagate through the weakest link in the microstructure. The grain boundaries or sub-grain boundaries are known to be weaker than the grains and hence the preferred crack propagation paths. The crack propagates along the α/β interfaces in the colony lamellar morphology and along the α′ needle interfaces in the fully martensitic morphology. Where sub-grains or laths are larger, cracks will be deflected less than in the finer structures. Within a colony morphology, a crack is deflected whenever it meets a differently oriented colony boundary. The deflection leads to crack branching and formation of secondary cracks. The coarser colony lamellar morphology leads to larger crack deflections than in the finer martensitic morphology. The larger the deflection of the crack (lower the crack growth) at α/β-phase interface or colony/grain boundaries, the rougher the fractured surface, as was found in the ST/FC specimen, while the smaller the deflection of the crack at a higher the crack growth rate at the α' interface or grain boundaries, the smoother the fractured surface, as in the ST/WQ specimen.

CONCLUSIONS

The correlation of microstructure and fatigue crack growth resistance in the Ti-6Al-4V alloy was investigated, and the following conclusions were drawn:

- The fatigue crack growth resistance was higher for the colony lamellar microstructure than for the fully martensitic morphology.
- The presence of α/β lamellar colonies led to crack deflection, branching, and formation of secondary cracks leading to high fatigue crack growth resistance.
- The fine martensitic needles in the fully martensitic microstructure did not hinder crack propagation.

FUTURE WORK

The results of the role of ageing treatment on the fatigue crack growth resistance were still being produced and will be included in future work.

LIST OF REFERENCES

Al-Bermani, S.S. et al., 2010. The Origin of Microstructural Diversity, Texture, and Mechanical Properties in Electron Beam Melted Ti-6Al-4V. *Metallurgical and Materials Transactions A*, 41(13), pp.3422–3434. Available at: http://link.springer.com/10.1007/s11661-010-0397-x.

ASTM E384, 2012. *Standard Test Method for Knoop and Vickers Hardness of Materials*, ASTM International, West Conshohocken, PA, USA.

ASTM Standard E647 − 13a, 2014. Standard Test Method for Measurement of Fatigue Crack Growth Rates. *American Society for Testing and Materials*, pp.1–50.

ASTM-E112, 2004. Standard Test Methods for Determining Average Grain Size 1. *Methods*, (July 1996).

Benedetti, M. & Fontanari, V., 2004. The effect of bi-modal and lamellar microstructures of Ti-6Al-4V on the behaviour of fatigue cracks emanating from edge-notches. *Fatigue and Fracture of Engineering Materials and Structures*.

Inagaki, I., 2014. Application and Features of Titanium for the Aerospace Industry. , (106).

Lütjering, G. & Williams, J.C., 2007. *Titanium* 2nd ed., Berlin, Heidelberg: Springer Berlin Heidelberg. Available at: http://link.springer.com/10.1007/978-3-540-73036-1.

Nalla, R.K. et al., 2002. Influence of microstructure on high-cycle fatigue of Ti-6Al-4V: Bimodal vs. lamellar structures. *Metallurgical and Materials Transactions A*, 33(13), pp.899–918.

Peters, C.L. and M., 2003. *Titanium and Titanium Alloys, Fundamentals and Applications*,

ACKNOWLEDGEMENTS

The authors would like to acknowledge the financial support of the Department of Science and Technology. Both the University of Pretoria and the CSIR are acknowledged for contributing and

giving permission to publish this work. The assistance and expertise of Chris McDuling is greatly appreciated in the production of fatigue crack growth results.

Author CV

Stephen Masete. Masters student at the University of Pretoria.

Stephen is on a masters studentship at CSIR Light Metals competency. He has a BSc degree in Chemistry from Wits University, a B Tech degree in Ceramics technology from Tshwane University of Technology and an Honours degree in (Applied Science) Metallurgy from the University of Pretoria. Stephen worked for Element Six research laboratory in Springs before coming to the CSIR for a studentship. He is currently completing MSc (Applied Science) Metallurgy with the University of Pretoria. The title of the masters topic is "The influence of ageing treatment on the microstructural evolution and the mechanical properties of the Ti-6Al-4V alloy".